Staple-Based Frequency Selective Surfaces for Electromagnetic Control in Buildings

Mariam Fawaz, Benito Sanz-Izquierdo, Edward.A. Parker

***Abstract*— This paper introduces a novel approach for using standard staples to create frequency selective surfaces (FSS) for controlling electromagnetic (EM) propagation within buildings. Single and dual polarized solutions are proposed in an initial configuration where off-the-shelf heavy-duty staples are arranged in a square lattice. Such design resonates at the widely used 2.4 GHz band with a -10 dB rejection bandwidth of about 20%. The design is stable to angle of incidence, particularly for leg lengths of over 0.026 λ. Parametric studies of the various dimensions and building material placement are included. An alternative design, featuring two staples arranged in a cross configuration, one placed directly on top of the other, operates at the 2.37 GHz band and offers improved angular stability and wider bandwidth, albeit with increased bulk. The resonant frequency of widely used staples in the two configurations is also provided, illustrating the ample possibilities. Simulations are confirmed experimentally. This work lays the foundation for the on-site deployment of staple FSSs as a durable, flexible solution to enhance the electromagnetic (EM) architecture of buildings.**

***Index Terms*, frequency selective surface (FSS), ultra-high Frequency (UHF), staple structures, EM propagation in Buildings.**

I. Introduction

FREQUENCY selective surfaces (FSS), also called spatial filters, are composed of a thin, repeating surface that changes the electromagnetic waves' absorption, transmission, or reflection based on the frequency of the electromagnetic field [1]. They typically comprise arrays of periodic conductors arranged on a dielectric material support [2]. While FSSs have traditionally been used in antenna radomes and radar systems, they have also been implemented in recent decades to control electromagnetic (EM) wave propagation and enhance the EM architecture of buildings [3]. By strategically incorporating FSS elements in building materials, such as walls [4] or windows [5], it is possible to shape and control the propagation of wireless signals. This can help improve signal strength, reduce signal leakage, and mitigate interference between different areas within buildings.

Manuscript received, May 2025.

The authors are with the School of Engineering, University of Kent, Canterbury, CT2 7NT, U.K. (e-mail: mf578@kent.ac.uk, b.sanz@kent.ac.uk, e.a.parker@kent.ac.uk).

In terms of applications of specific FSS types, patch-type band-stop FSSs can be used to suppress unwanted frequencies or improve coverage by reflecting or redirecting signals [6]. On the other hand, slot-type band-pass FSSs can reject most frequencies while allowing transmission at a specific frequency [7]. Even with a small number of elements, band-pass FSSs [8] can enable communication within designated bands while blocking others, making them suitable for use in secured rooms.

Regarding fabrication techniques, both traditional and more recent additive manufacturing methods have been employed for FSSs in building applications. Traditional fabrication methods are limited by the need for specialized workshop equipment, such as chemical etching setups or milling machines for track removal. Additive manufacturing techniques used for fabricating FSSs include inkjet printing [9], aerosol jet printing [10], and even full 3D printing [11], [12]. Planar printed FSSs have been implemented in walls in the form of wallpaper [13], and FSSs have also been printed directly onto plasterboards using screen printing techniques [14]. While these printing techniques are well-suited for prototyping, they are not easily adaptable or adjustable on a building site.

FSS designs for building applications come in various shapes and sizes, but most are based on 2D or planar configurations. Another category that could be suitable for buildings is the 3D FSS. Compared to 2D designs, 3D FSSs may offer enhanced bandwidth, greater frequency selectivity, improved performance over a range of incident angles, reduced losses in tunable configurations and polarization conversion for incident waves. Previous work on 3D FSS designs has primarily involved manually inserted mechanical elements [15] – [19]. One example is a spring-loaded FSS [15], where adjusting the height of the mechanical spring allows for tuning the resonant frequency and switching between band-stop and band-pass operations. A 3-D mechanically tunable FFS based on moving the internal patch in square slot FSS is discussed in [16]. Such structure offers low insertion losses, a narrower relative bandwidth, and adjustable resonant frequency with a tuning range of about 50%. In [17], a 3D FSS using helical shapes is able converts linear polarization to circular polarization in the 28 to 31 GHz frequency range. A more complex 3-D FSS based on a two-dimensional (2-D) array of shielded microstrip lines with shorting via to ground achieves wide out-of-band rejection by incorporating multiple transmission zeros is presented in [18]. Another 3D design, in this case based on folding loop elements is described in [19]. The design reduces the resonant frequency and improves the angle of incidence by folding in the third dimension. It employes 3D printing for the elements of the array and materials typically used in buildings. These reviewed

(a) (b)

Fig. 1 Illustration of the on-site implementation of a staple-based FSS: a) staple FSS placement with staple gun, b) operation of staple-based FSS wall.

3D FSS structures have limitations due to the manual placement of elements, slow fabrication process and not real consideration for on-site development and implementation such as in a building.

This paper introduces the concept of using off-the-shelf staples to create frequency selective surfaces for building applications. Heavy Duty staples are investigated for the development of FSSs. Two potential configurations are proposed. In the first one, standard staples are arranged on a square lattice to create single or dual polarized FSS designs. The FSS resonates at the widely used 2.45 GHz frequency band with a -10 dB bandwidth of 20% when placed on a cardboard substrate. Parametric studies provides the resonant frequency and performance for various changes in the staple size as well as placement on potential building materials. A second dual polarized configuration where the staples cross on top of each other is also proposed. Such configuration also covers the 2.4 GHz band and provides improved angular behavior to incident waves. A table with the resonant frequency for commonly used staples is included for future reference and potential practical implementations. These designs offer practical applications in the context of buildings, as they can be incorporated into walls using a staple gun as illustrated in Fig 1. They possess several advantages, such as rapid on-site deployment, durability, compatibility, flexibility, and uniqueness compared to previously reported FSS design suitable for building applications. All designs and simulations were carried out using CST Microwave Studio ™.

The paper is organized as follows. Section II introduces the first FSS staple configuration and analyses its performance. Section III describes a second FSS design consisting of on-top cross staples. Section IV provides the operational frequency of various available staples when arranged on the proposed configurations. It also compares the designs with previously reported 3D FSS designs. Finally, section V summarizes the work and provides a conclusion.

II. Single and Dual Polarized Staple FSS Concept

A. Staple FSS Design

A staple is a metallic material widely used in building, packing and office applications. A typical staple consists of a crown with two perpendicular legs. Staples come in many sizes depending on the application. Heavy-duty staples are used in construction for tasks such as installing paneling, laying floors, and similar applications due to their thick gauge, strong penetration, and durable steel construction.

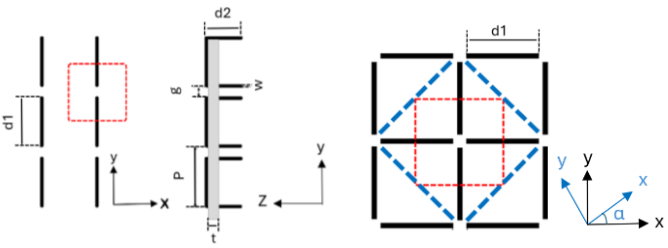

(a) (b) (c)

Fig. 2 Structure of single polarized staple based FSS: a) Front view of element with unit cell in red, b) Side view of single polarized, c) Front view of Dual polarized with unit cell for 0º degrees polarization rotation (red) and 45º polarization rotation with second potential unit cell (blue).

Table I
Dimensions for the Staple FSS.

Parameter	d_1	d_2	p	t	g	w
Value (mm)	25.4	19	30	4	4.6	1.5

d_1: Crown length, d_2: Leg length, p: Periodicity, t: thickness of the substrate, g: distance between staples, w: staple width.

They are readily available and are typically implemented using manual or automatic equipment. Thus, they can be an attractive solution for on-site modification of the electromagnetic architecture of buildings (Fig.1).

The first design, which arranges staples into FSS, and supports both single and dual polarization, is shown in Fig 2. Arrows HT-65's heavy-duty staples [20], made of steel galvanized with Zinc, with dimensions listed in Table I, were arranged in a square lattice of periodicity, p, of 30 mm. The staple resembles a typical dipole FSS array when looking from the front (Fig. 2(a)). Fig. 2(b) presents the side of the array when placed on a thin substrate, showing the legs inserted in a supporting substrate. The substrate employed corresponds to cardboard with a thickness of 4 mm, a dielectric constant (ε_r) of 1.78, and loss tangent (tan δ) of 0.025 [21]. Zinc was used as the material for the staples in simulations.

Additional staples can be placed at the edge of the square cell and perpendicular to the vertical staples to create a dual polarized design as shown in Fig. 2(c). The design was simulated as a unit cell within an infinite array, indicated by red dashed lines. Angular rotation for the incidence polarization can be important in building applications due to multipath effects. This is presented by α, illustrating the case when the rotation angle is 45º, which can be directly adjusted in simulation. For reference, a potential stand-alone unit cell corresponding to the 45º rotation angle is shown in blue dash line in Fig. 2(c). Simulations were carried out as infinite unit cell.

Figure 3 shows the simulated responses of the single and dual polarized FSS designs at various angles of incidence: normal (0º), TE45, and TM45, as well as rotation angles. The singly polarized FSS (Fig. 2(a)) resonates at 2.45 GHz at normal incidence, with a frequency shifting of about 1% for both TE45˚ and TM45˚. The dual-polarized FSS (Fig. 2(c)) resonates at 2.42 GHz under normal incidence at a 0° rotation angle, with frequency shifts of less than 1% at TE45° and TM45° (Fig. 3(b)).

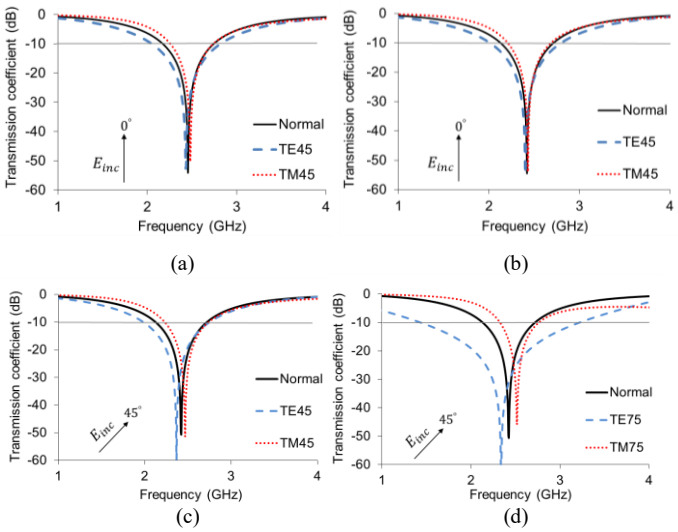

Fig. 3 Simulated transmission responses for the staple FSS: a) singly polarized staple based FSS, (b) dual polarized at 0° rotational angle, (c) dual polarized design at 45° rotational angle; (d) dual polarized design at 45° rotational angle and 75° incident angles.

At 45º rotational angles (Fig. 3(c) and Fig. 3(d)), the resonant frequency remains constant at 2.42 GHz under normal incidence, but shifts further with increasing rotational angle at TE45˚ and TM45˚. In Fig.3(c), the largest shift is observed for 45° rotation, with shifts in TE45˚ and TM45˚ of 2% and 1.6% respectively. For large angles of incidence, such as 75° (Fig. 3(d)), the frequency shifts are 4% at TE75 and 3.3% at TM75, with the filtering response becoming significantly broader at TE75. Overall, the dual band design covers the -10 dB bandwidth from 2.21 GHz to 2.73 GHz, accounting for all assessed angles, and even for larger angles such as 85º, which is within the commonly used 2.4 GHz wireless band.

The surface current distribution for the singly and the dual polarized staple FSS when illuminated by an incident wave with E-vector in the y-direction are shown in Fig. 4. For the singly polarized design, maximum currents can be observed at the center of the staple and minimum currents at the edge of the legs. A similar current distribution is seen for the vertical elements in the dual polarized FSS (Fig. 4 (b)) with minimal currents in the horizontal staples. When the dual polarized design is rotated by 45° (Fig. 4(c)), maximum currents occur at the centers of all diagonal staples, with minimum currents at the edges of the legs.

Currents in the staple in Fig. 4 (a) and (b) are similar to those of the square loop FSS in Fig. 4(d), which consists of two mirrored dipole (or staple) elements connected in the middle.

B. Equivalent Circuit

The equivalent circuit model (ECM) of the staple FSS can be derived from the square loop as illustrated in Fig. 5. The square loop can be split in the middle (Fig. 5 (a)) and then folded to the back to create the staple Fig. 5 (b).

For the square loop FSS, the approximate inductance and capacitance is typically calculated using the following equations [22], [23], [24]:

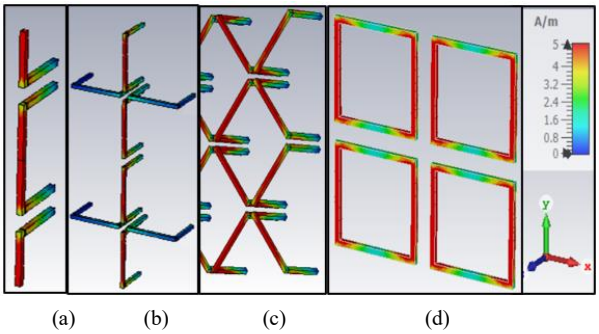

Fig. 4 Surface current distributions: (a) singly polarized FSS (b) dual polarized FSS at 0° rotation angle. (c) dual polarized FSS at incidence rotation angle of 45°, (d) square loop FSS.

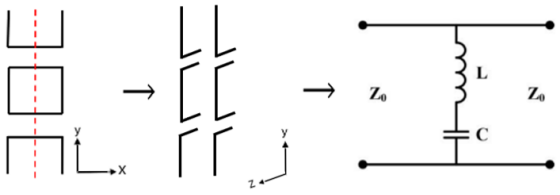

Fig. 5 Development of equivalent circuit for the staple FSS: (a) square loop (b) staple FSS (c) equivalent circuit model (ECM).

Table III
ECM values and corresponding resonant frequency for varying d_2.

d_2 (mm)	C (pF)	L (nH)	f calculated (GHz)	f simulated (GHz)
3	0.158	6.25	5.06	5.08
19	0.315	12.55	2.53	2.56
30	0.417	16.66	1.91	1.86
50	0.656	26.63	1.21	1.23
100	1.17	47.55	0.675	0.675

$$C = \varepsilon_0 \varepsilon_{eff} \frac{2D}{\pi} \log\left(\frac{1}{\sin\frac{\pi S}{2D}}\right) \quad (1)$$

$$L = \mu_0 \frac{D}{2\pi} \log\left(\frac{1}{\sin\frac{\pi w}{2D}}\right) \quad (2)$$

$$\omega = \frac{1}{\sqrt{LC}} \quad (3)$$

where ε_0 and μ_0 are the permittivity and permeability of the free space, *P* is the periodicity of the unit cell, w is the width of the square loop and *S* are the separation distance between the loop and *D* is the length of the side of the square loop.

By cutting and rotating the loop to form the staple, a new variable, leg length d_2 (Fig. 2), is introduced alongside side length d_1 (Fig. 1, Table I). This requires adjusting the ECM using the following equation for *D*:

$$D = 0.2d_1 + 0.47d_2 \quad (4)$$

(4) produces independent values of *C* in (2) and *L* in (3) and then resonant frequency from (3) which matches simulations

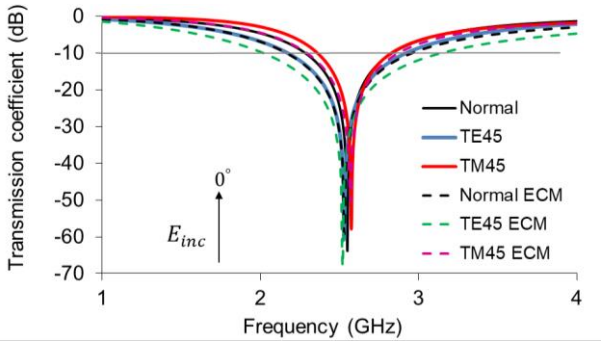

Fig. 6 Simulation transmission coefficients for the CST simulations and the ECM model using ADS for the single polarized staple FSS in free space.

with a deviation of less than 3% in free space (no substrate) for values of d_2 less than 1.2 d_1, as presented in Table II, for d_2 from 3 mm (0.16 d_1) to 30mm (1.2 d_1), with 19 mm corresponding to the staple used in practical experiments.

For d_2 of over 1.2d_1, the resonant frequency of the ECM starts to deviate from simulations. The reason for this is that the capacitive component due to d_2 becomes significantly more predominant in the ECM circuit than d_1. In this case, (4) needs to be adjusted to:

$$D = 0.0787d_1 + 0.6d_2 \tag{5}$$

(5) has been verified for d_2 values between 1.3d_1 and 5d_1, with less than 2% deviation between the ECM circuit resonance and simulations, as shown in Table II for 2d_1 (50 mm) and 4d_1 (100 mm). The equation may still apply for higher d_2/d_1 ratios, though with increased error. However, staples with d_2/d_1 ratios above 5 are uncommon.

When evaluating the ECM for oblique incidence, the expressions for capacitance and inductance should be modified to consider the change in theta at both TE and TM polarization. The following equations can be used to calculate the capacitance and inductance at different oblique incidence angles, and accordingly, to determine the resonance frequency of the FSS design [25], [26]:

$$C_{TE}(\theta) = C_{TE0}\left(1 - \frac{k_0^2}{k_{eff}^2}\frac{sin^2(\theta)}{\alpha}\right) \tag{6}$$

$$L_{TM}(\theta) = \frac{L_{TM0}}{\left(1 - \frac{sin^2(\theta)}{\alpha}\right)} \tag{7}$$

The value of α in these equations is element dependent, and for the staple FSS, the estimated values are approximately −62.3 for TE polarization and −24.6 for TM polarization. This provides resonant frequencies with a deviation of less than 1% from CST simulations for angles between 0° and 60° for both TE and TM incidence. Fig. 6 shows the comparison between the transmission response from CST simulations and that of the ECM model simulated using Agilent Design Software (ADS). The ECM model provides consistent transmission results both at normal incidence and for varying angles of incidence.

Note that further studies will be required for the ECM for different substrates and thicknesses. This can be considered by obtaining effective permittivity of the substrate and then inserting it into (1).

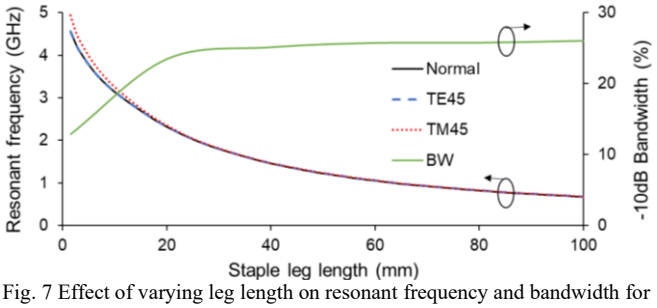

Fig. 7 Effect of varying leg length on resonant frequency and bandwidth for the dual polarized FSS.

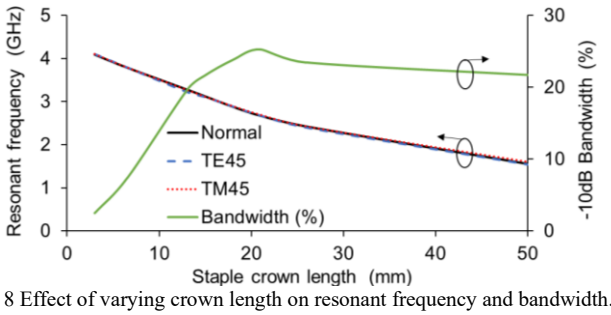

Fig. 8 Effect of varying crown length on resonant frequency and bandwidth.

C. Parametric Analysis for potential inbuilding staples FSS.

The staple could be considered as a folded half-wavelength dipole element with approximate resonant frequency in free space and without substrate:

$$f = \frac{c}{2(d_1+2d_2)} \tag{8}$$

where c is the speed of light and d_1 and d_2 are the crown and leg length of the staple in meters. However, the resonant frequency will vary differently depending on each parameter of the staple as well as the substrate characteristics.

The staple length, crown length, leg bending angle when inserted and substrate characteristics and thickness are the main parameters considered in this study. For the analysis, these parameters have been varied independently while keeping the other parameters as given in Fig. 2 and Table I. These studies focus on large arrays that could be applied to walls in buildings, where the infinite unit cell approximation applies.

The effect of varying the staple's leg length, d_2, from 1.5 mm (effectively no leg) to 100 mm on the resonant frequency and -10 dB bandwidth is shown in Fig.7. There is a rapid decrease in resonant frequency from 1.5 mm to about 30 mm (d_2 < 1.2 d_1), followed by a slower pace from about 40 mm to 100 mm (d_2 = 4 d_1). This trend is consistent with (4) and (5) and the ECM. The angle of incidence performance also improves with increasing leg length. The -10dB bandwidth initially increases rapidly, reaching 22% at about 20 mm, and then grows more gradually from 20 mm to 100 mm, where it reaches 25%.

The effect of changing the size of the crown, d_1, between 3 mm to 50 mm on the resonant frequency is shown in Fig.8. The frequency decreases continuously from around 4 GHz to 1.5 GHz, while performance at TE45 and TM45 angles of incidence degrades as the crown length increases. For a crown length of 3 mm which is effectively a horizontal wire, the -10 dB bandwidth is just 2.5%. The bandwidth then increases rapidly to a maximum of 25% for 21mm crown length and then decreases very slowly from 25 mm to around 21% for 40 mm.

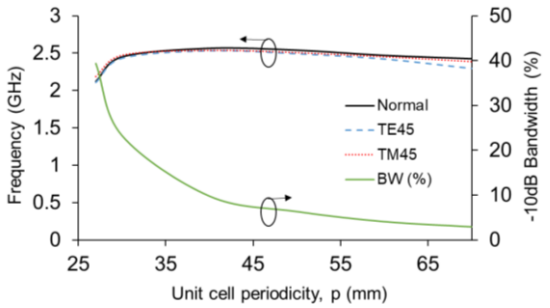

Fig.9 Effect of varying the periodicity, p, while keeping the dimensions of the staple constant.

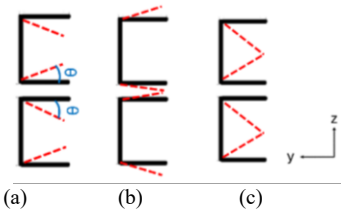

Fig. 10 Effect of leg bending: a) legs showing the bending angle, b) legs touching to the outside, (c) legs touching to the inside.

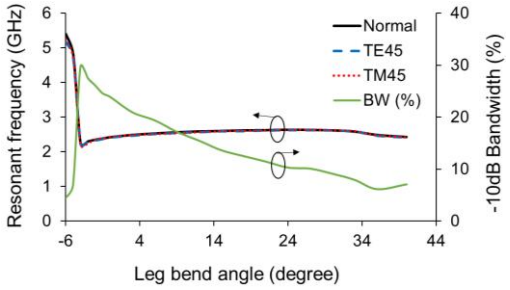

Fig. 11 Effect of leg bending angle on resonant frequency.

The effect of varying periodicity, *p*, with staple dimensions fixed, is shown in Fig. 9. When the staples are placed very close to each other, the resonant frequency is lowest (2.2 GHz) and the bandwidth is highest (40%). As *p* increases, the bandwidth decreases rapidly. The resonant frequency, on the other hand, rises to 2.5 GHz at 45 mm, then gradually falls to 2.3 GHz at 70 mm. A useful rejection bandwidth across all described incidence angles is maintained up to approximately 60 mm.

When inserting the staples into a surface, the legs might bend to some degree, as illustrated in Fig. 10. Depending on the direction of bending, the legs may either spread apart (Fig. 10(a)), approach and even touch adjacent staples (Fig. 10(b)), or bend inward until they touch within the same staple (Fig. 10(c)). Fig. 11 shows the effect of this leg angle on the resonant frequency and bandwidth. When the legs of adjacent staples bend toward each other (negative angle), the resonant frequency decreases. However, once the legs make contact (Fig. 10(b)), the resonant frequency abruptly increases, nearly doubling to around 5 GHz. Conversely, when the legs bend inward (Fig. 10(a)), the resonant frequency gradually increases, reaching approximately 2.6 GHz at an angle of 30°. Beyond this point, as the angle continues to increase to 40° and the legs touch internally (Fig. 10(c)), the frequency decreases slightly to around 2.4 GHz. In terms of -10 dB bandwidth, it is 5% when the legs are touching adjacent staples. As the legs begin to separate, the bandwidth increases sharply, peaking at 30% near -4°, and then gradually decreases to 7% at 40°.

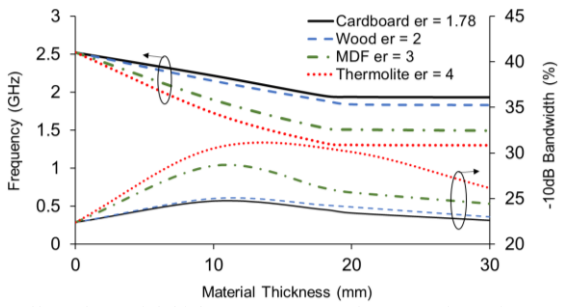

Fig. 12 Effect of material thickness on resonant frequency for various materials.

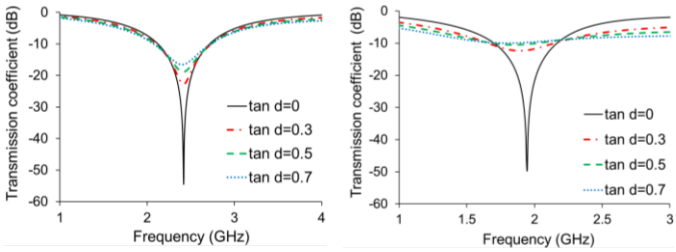

Fig. 13 Effect of varying loss tangent on the transmission response: (a) cardboard (εr = 1.78) with thickness (t = 4 mm), (b) cardboard substrate thickness (19.05 mm).

Overall, minor bending of the legs has limited impact on performance. Furthermore, in real scenarios, there would probably be a mixture of the various bending directions.

The effect of the surrounding building materials is also of significant interest if the FSS is to be used in buildings [27], [28]. Fig. 12 illustrates the effect of changing the thickness of the substrate on S_{11}, considering both the thickness and type of supporting material. The study uses the permittivity values of various common building materials, including cardboard [21], wood [29], medium-density fibreboard (MDF) [30], and Thermolite [30]. As the substrate thickness increases, the resonant frequency decreases until the substrate fully covers the legs of the staples. Beyond this point, the resonant frequency remains constant. This trend is observed across all materials; however, the rate of frequency change is more pronounced for materials with higher permittivity. The -10 dB bandwidth increases with substrate thickness up to the length of the staple legs and then begins to decrease. These bandwidth variations are also more significant in materials with higher permittivity.

Building materials may introduce electrical losses due to fabrication imperfections or exposure to water and humidity, which can affect the performance of the FSS. The effect of increasing the loss tangent in a carboard substrate of 4 mm and 19.05 mm thickness is shown in Fig 13(a) and Fig. 13(b) respectively. As the loss tangent increases, the resonance broadens, and the depth of the transmission null decreases. This indicates that materials with higher losses reduce the FSS's efficiency, leading to poorer frequency filtering and a lower Q-factor. The impact of material losses on transmission is more pronounced when the staples' legs are fully covered by the dielectric. Therefore, in areas with high material losses or humidity, it is recommended to use thinner supporting materials, waterproof substrates and superstrates, or to coat the surface with anti-damp paint or a similar protective coating.

Note that changing the material of the staple from zinc to other material can modify the depth of the transmission null.

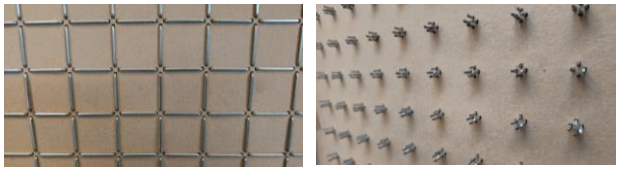

(a) (b)

Fig. 14 Staples inserted on the cardboard substrate: (a) front, (b) back view.

(a) (b) (c)

Fig. 15 Fabricated staple FSS: (a) singly polarized, (b) dual polarized, (c) rotated.

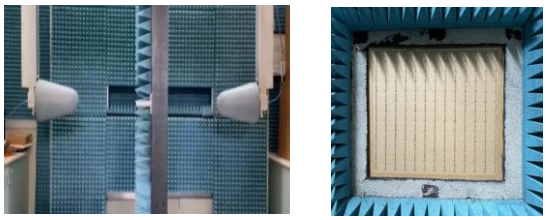

(a) (b)

Fig. 16 Measurement set up: (a) side view, (b) FSS in the center of the aperture.

Materials with higher conductivity, such as copper, can increase the depth of the null by 5 dB, while lower-conductivity materials like steel may reduce the depth by about 4 dB.

D. Fabrications and measurements

To fabricate the staple FSS, a finite array of 13 by 13 staples was created, and the position of the staples' legs were exported to a .dxf file. Two 2 mm thick cardboard sheets were then laser cut with holes matching the staples' legs positions, along with a 45 mm by 45 mm outline.

The standard 25.4 mm by 19 mm (1 in by ¾ in) staples for HT-65 Hammer tacker were employed [20]. The frequency-selective array was crafted by carefully inserting the staples within laser-cut apertures on a cardboard support. The two layers of laser-cut cardboard material were attached together for a total thickness of 4 mm. This was required to provide sufficient mechanical robustness and avoid misalignments or unwanted movement of the staples. Fig. 14 displays the front and back of the staples inserted on the cardboard for the dual polarized design. Three designs were fabricated for this staple FSS array, the singly polarized (Fig. 15(a)), the dual polarized (Fig. 15(b)), and the 45º rotation FSS design (Fig. 15(c)). Note that the rotational FSS design was fabricated for the purpose of assessing it as a standalone FSS. However, the 45° rotation could also be assessed by directly rotating the dual polarized design.

Fig. 16 shows the measurement set up with the transmitted antenna and the panel fitting the FSS positioned in the center. The setup was arranged in a test chamber divided into two halves by a rotatable screen lined with microwave absorbers,

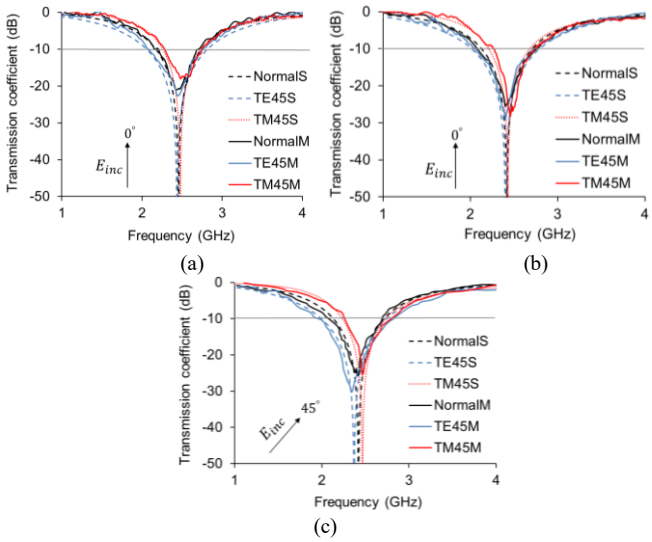

Fig. 17 Measurement and simulation transmission response for staple FSS: (a) Singly polarized design, (b) dual polarized design, (c) Rotated design.

allowing for angle of incidence transmission measurements. The screen featured a centrally adjustable aperture designed to hold the FSS under test. Both the transmitting and receiving antennas were positioned 1 meter from the aperture, as shown in Fig. 16(a). A Marconi Instruments® Microwave Test Set 6204B was used to measure the transmission response of the FSS in the plane wave chamber.

The measured transmission responses for the three prototypes, under normal incidence TE45˚ and TM45˚, are presented in Fig. 17. In all three staple FSS configurations, the resonance occurred at about 2.4 GHz. For the singly polarized FSS, the resonance was observed at 2.42 GHz under normal incidence, with frequency shifts of 1% at TE45˚ and 2.5% at and TM45˚. For the dual polarized FSS at 0 rotational angle, the resonance occurred at around 2.4 GHz at normal incidence, with frequency shifts of less than 1% at TE45 and 2% at TM45. Finally, for the dual polarized at 45º rotational angle, resonance occurred at 2.41 GHz under normal incidence with frequency shifts of about 3% at both TE45 and TM45. Note that the measured resonant frequencies differ from the simulations by less than 5%, likely due to fabrication and placement errors. In particular, slight variations in the spacing between the legs at the ends of the staples were observed, as shown in Fig. 14(b). Nevertheless, the FSS successfully covered the target 2.45 GHz band with approximately 24% -10 dB bandwidth.

III. ON-TOP CROSS STAPLE FSS CONFIGURATION

A. Design, fabrication and results

Another design to consider when using staples is placing one staple perpendicular and on top of another as illustrated in Fig.18. Although this may have some limitations, such as some staples popping up, it could still be practical for use with softer materials such as wood. Thus, the design is described briefly in this section. The dimensions of the FSS structure are given in Table III. Notably, this approach allows for a smaller unit cell size compared to the design in the previous section.

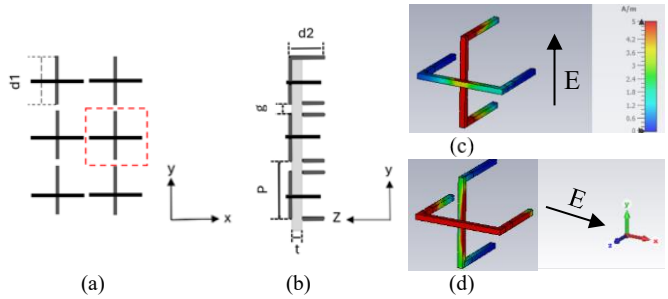

Fig. 18 On top cross staple design: (a) front view of element with unit cell in red, (b) side view, (c) surface currents when vertically polarized, (d) surface currents when horizontally polarized.

Table III
Dimensions of the on Top Cross Staple FSS.

Parameter	d_1	d_2	p	t	g	w
Value (mm)	25.4	19.05	28.4	4	3	1.4

d_1: Crown length, d_2: Leg length, p: periodicity, t: thickness of the substrate, g: distance between staples, w: staple width.

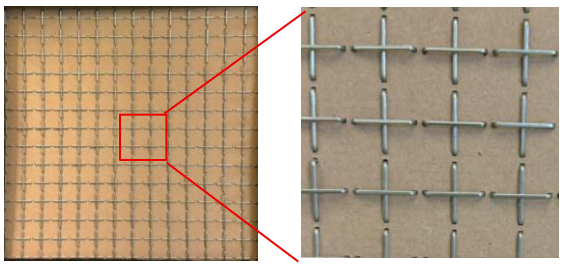

Fig. 19 On top cross staple design (a) full array, (b) zoomed in view.

The surface current distributions for the FSS when excited by a vertical E-field and a horizontal E-field are shown in Fig. 18(a) and Fig. 18(b), respectively. Currents are maximum at the center of the staple being excited by the corresponding incident wave with minor currents extending to the other staple.

The same fabrication process was used for the top cross design, with the staples placed in the laser cut holes to create the 13 by 13 shown in Fig. 19.

The FSS was simulated and measured at both 0° and 45° rotational angles for the two polarizations, with the transmission responses shown in Fig. 20. In the simulations, the FSS resonated at approximately 2.36 GHz, with frequency shifts of less than 1% for both TE45° and TM45° across all cases. Specifically, when the E-field was vertical (Fig. 18(c)), the FSS resonated at 2.37 GHz under normal incidence, 2.35 GHz at TE45°, and 2.37 GHz at TM45° (Fig. 20(a)). When the E-field was horizontal (Fig. 18(d)), the FSS resonated at about 2.36 GHz under normal incidence and TM45°, and 2.35 GHz at TE45° (Fig. 20(b)). For 45° rotational angles relative to the vertical (Fig. 20(c)) and horizontal polarization (Fig. 20(d)), the FSS resonated at approximately 2.37 GHz for both normal incidence and TE45°, and 2.35 GHz at TM45°.

The measured results, also shown in Fig. 20, agree well with the simulations. The main resonant frequency was approximately 2.36 GHz, with a −10 dB bandwidth of 25% across all measured angles. The frequency shifts for TE45° and TM45° were slightly over 1%. For the 45° rotational angles

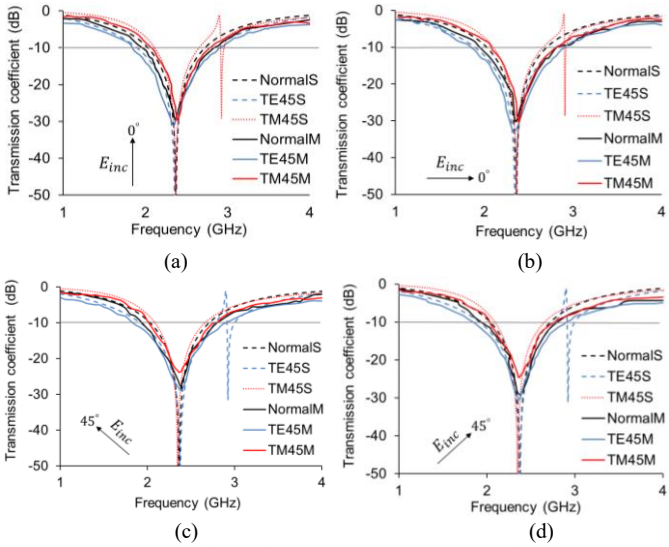

Fig. 20 Measurement and simulation transmission response for on top cross staple FSS (a) E-field vertical and 0° rotational angle, (b) E-field horizontal and 0° rotational angle, (c) E-field vertical rotated by 45°, (d) E-field horizontal 45°.

Table IV
FSS Performance of Various Staples.

Name	d1 (mm)	d2 (mm)	w_1 (mm)	w_2 (mm)	p_s (mm)	p_x (mm)	fs (GHz)	fx (GHz)
6/4	7.1	4.2	0.35	0.5	8	7.57	8.75	8.31
No.10	9.4	4.65	0.35	0.5	10.5	9.94	6.94	6.61
26/6	12.8	6	0.4	0.5	14	13.2	5.14	4.42
26/8	12.8	8	0.4	0.5	14	13.2	4.53	3.99
23/10	13	10	0.5	0.75	14	13.2	3.99	2.37
23/25	13	25	0.55	0.75	14	13.2	2.24	1.74
25/19	25.4	19.05	1.4	1.4	30	28.4	2.42	2.37

fs: Frequency of staple
fx: frequency of cross staple

(Fig. 20(c) and (d)), the resonant frequency was about 1% lower than in the simulations. A spike appears in simulations at 2.9 GHz for both TM 45° at 0° rotational angle and TE 45° at 45° rotational angle, but it is not observed and has no effect in measurements due to its very narrow bandwidth. This behavior is typical of cross dipole structures, where the dipoles intersect at the center, creating multiple current paths, especially under oblique incidence.

The differences between simulations and measurements were likely due to manual placement of the staples, where the spacing between the legs was not fully consistent throughout the array.

IV. Discussion and Conclusions

A. Discussion

Staples are available in various sizes depending on the application, and each size resonates at a different frequency. This characteristic can be useful for controlling wave propagation in buildings. Table IV presents the resonant frequencies of several commonly available staples when arranged in the lattice configurations described in this paper.

Table V
Comparison of 3D FSS Designs.

FSS	p/λ / type	Center frequency (GHz)	Bandwidth: 3dB band pass / -10dB band stop (%)	Loss (dB)	Main features: polarization, material, cost
Ref [15]	Bandstop: 0.41 x 0.41 Bandpass: 0.45 x 0.45	3.43 3.53 3.63 ≈3.18 ≈3.5 3.76	≈2.33 ≈1.42 ≈1.10 ≈5.66 ≈3.8 ≈2.66	<1	Singly polarized Stacked springs Mechanical tunable High cost
Ref [16]	Bandpass: 0.28 x 0.28	0°: 2.41 45°: 2.16 90°: 1.98	0.195 0.240 0.29	<3	Singly polarized Mechanical tunable patches Medium cost
Ref [17]	Bandstop: 0.11 x 0.11	27	15	-	Singly polarized Millimeter wave polarizer High cost
Ref [18]	Band pass: 0.47 x 0.47 0.25 x 0.25	8 8.2	34 17.5	0.8 1.2	Singly polarized Mechanical plates and microstrips Medium cost
Ref [19]	Bandstop 0.21 x 0.21	2.5	24	<2.0	Single/Dual polarized 3D printing /folded elements High cost
This work	Bandstop Flexible 0.24 x 0.24 to 0.067x0.067	Single: 2.54 Dual: 2.42 Cross: 2.36	20 20 25	<1.0	Single/Dual polarized Off-the-shelf staples Flexible Durable Low cost

The table includes the staple names along with their key dimensions: crown width, leg length, and thickness. A wide range of operational frequencies, from approximately 1.7 GHz to 9 GHz, can be achieved by selecting appropriate staples. For staples not listed, an initial estimate of the resonant frequency can still be obtained using (6) and taking in consideration the effect of material placement in section II. C (Fig. 13).

A comparative analysis of the proposed FSS design and previously reported 3D FSS structures is presented in Table V. Most of the designs listed in the table offer distinct and innovative features. Although many include components that extend along the z-axis, none make use of off-the-shelf staples or explore the design flexibility they offer. For instance, the periodicity of a staple-based FSS relative to the operational wavelength can be adjusted primarily through the leg length of the staple. In terms of fabrication costs, the use of staples offers a lower fabrication cost compared to the other methods discussed. In this work, the staples used result in a normalized periodicity (p/λ) of about 0.24 by 0.24. However, using a similar staple inserted into cardboard with a leg length equal to half the typical wall thickness, or approximately 100 mm, can yield a much smaller normalized periodicity, around 0.067 by 0.067. It maintains a normalized bandwidth of up to 20 - 25% with insertion loss below 1 dB, which is on par with or better than many mechanically tuned or 3D-printed alternatives that often exhibit higher losses or narrower bandwidths.

Another key advantage of the proposed approach is its enhanced design flexibility. For instance, staples can be arranged to achieve single, dual, or other types of polarization by adding, removing, or orienting them as needed. Although only two configurations have been presented in this paper, many other arrangements can be created using the same technique to produce transmission responses tailored to specific applications. Additionally, staples can be selected based on their resonant frequencies, as shown in Table IV, or combined to enable multiband operation.

In terms of fabrication, the 3D FSS designs listed in the table generally involve challenges and require various methods such as 3D printing [19] or complex mechanical processes [15]–[18]. These methods can be expensive and time-consuming. In contrast, the staple-based FSS can be easily implemented by using an automatic staple gun to insert staples into building materials. This approach can also be adapted to an x-y robotic system for rapid and cost-effective deployment. Furthermore, it may be considered a more sustainable alternative to standard etching used in planar structures, as it avoids subtractive manufacturing processes and results in less material waste.

B. Conclusion

This work has proposed the concept of using off-the-shelf mechanical staples to create novel frequency selective surfaces (FSSs) for building applications. Both singly and dual-polarized staple FSSs were demonstrated, resonating around the 2.45 GHz band commonly used in indoor wireless communications. An equivalent circuit model has been validated against full-wave simulations, showing good agreement and providing a useful tool for fast initial design and analysis of such structures. A stacked-staple configuration was also explored, enabling a denser array and slightly lower resonant frequency. Staple-based FSSs offer good angular stability and high design flexibility, with a large choice for resonant frequencies and transmission characteristics. Very low resonant frequencies can be achieved using staples with longer legs.

Due to their simplicity and adaptability, staple FSSs are well suited for integration into building materials to manage electromagnetic wave propagation, such as filtering or reflecting signals in targeted areas. Such integrations are useful for improving indoor signal integrity, reducing interference

from external wireless sources, and enabling secure or controlled wireless communication environments particularly in smart buildings, data centers, and secure facilities. Although staples were manually inserted in this study, future implementation using automated staple guns and x-y robotic systems is envisioned, enabling accurate, scalable, and cost-effective deployment. This method may also offer a more sustainable alternative to traditional FSS fabrication by reducing material waste. To improve the accuracy of ECM model predictions, future work may incorporate higher-order corrections or machine learning regression techniques. Angular stability, particularly at high incidence angles, could be further enhanced by introducing a dielectric superstrate. Additional research will explore multi-staple layered lattices and hybrid geometries that combine different staple sizes or layouts to improve filtering performance and design flexibility. Furthermore, tunable or reconfigurable designs may be investigated using electronic or responsive materials that adapt the structure in response to external stimuli such as heat or electrical current.

REFERENCES

[1] A. Munk, *Frequency Selective Surfaces: Theory and Design*, 1st ed. New York, USA:Wiley, 2000.

[2] E. A. Parker, *The Gentleman's Guide to Frequency Selective Surfaces.* Kent Academic Repository [Online]. Available: http://kar.kent.ac.uk/59863/.[Accessed: Apr. 16, 2025].

[3] M. Philippakis, C. Martel, D. Kemp, R. Allan, M. Clift, S. Massey, S. Appleton, W. Damerell, C. Burton, and E. A. Parker, *Application of FSS Structures to Selectively Control the Propagation of Signals into and out of Buildings*, Ofcom, Tech. Rep. AY4464A, 2003.

[4] M. Raspopoulos and S. Stavrou, "Frequency Selective Buildings Through Frequency Selective Surfaces," *IEEE Trans. Antennas Propag.*, vol. 59, no. 8, pp. 2998-3005, Aug. 2011.

[5] A. A. Dewani, S. G. O'Keefe, D. V. Thiel and A. Galehdar, "Window RF Shielding Film Using Printed FSS," *IEEE Trans. Antennas Propag.,* vol. 66, no. 2, pp. 790-796, Feb. 2018.

[6] P. Callaghan, P. Giannakou, S. G. King, M. Shkunov and P. R. Young, "Linearly Polarized Reconfigurable Reflect array Surface," in *IEEE Trans. Antennas Propag.*, vol. 69, no. 10, pp. 6480-6488, Oct. 2021.

[7] B. Sanz-Izquierdo, E. A. Parker, J. -B. Robertson and J. C. Batchelor, "Singly and Dual Polarized Convoluted Frequency Selective Structures," , *IEEE Trans. Antennas Propag*., vol. 58, no. 3, pp. 690-696, March 2010

[8] E. A. Parker, A., J.-B Robertson, B. Sanz-Izquierdo, J. C. Batchelor, "Minimal Size FSS for Long Wavelength Operation", *IET. Electronics Letters*, 44 (6). pp. 394-395.,2008.

[9] B. M. Turki, E. A. Parker. Sebastian Wünscher, Ulrich S. Schubert, Rachel Saunders, Veronica Sanchez-Romaguera, Mohamad Ali Ziai, Stephen G. Yeates, and John C. Batchelor., "Significant Factors in the Inkjet Manufacture of Frequency-Selective Surfaces," *IEEE Trans. Compon., Packag. Manuf. Technol.,* vol. 6, no. 6, pp. 933-940, June 2016

[10] A. Shastri et al., "3D Printing of Millimetre Wave and Low-Terahertz Frequency Selective Surfaces Using Aerosol Jet Technology," IEEE Access, vol. 8, pp. 177341-177350, 2020,

[11] S. Ghosh and S. Lim, "A Miniaturized Bandpass Frequency Selective Surface Exploiting Three-Dimensional Printing Technique," *IEEE Antennas Wireless Propag. Lett.*, vol. 18, no. 7, pp. 1322-1326, July 2019.

[12] A. Shastri, B. Sanz-Izquierdo, A. Elibiary and E. A. Parker, "Manufacturing, Developments, and Constraints in Full 3-D Printing of Frequency-Selective Surface Using Low-Cost Open-Source Printer," *IEEE Trans. Compon., Packag. Manuf. Technol.,* vol. 11, no. 12, pp. 2193-2200, Dec. 2021,

[13] A. Shastri, P. Njogu, B. Sanz-Izquierdo, S. Gao and Z. Chen, "Low-cost Inkjet Printed Paper Poster FSS for 5G Applications," *2021 15th European Conference on Antennas and Propagation (EuCAP)*, Dusseldorf, Germany, 2021, pp. 1-4, doi: 10.23919/EuCAP51087.2021.9411448.

[14] P. Njogu, A. Shastri, A. Smith, S. Gao and B. Sanz-Izquierdo, "Screen-Printed FSS Plasterboard for Wireless Indoor Applications," *2022 Microwave Mediterranean Symposium (MMS)*, Pizzo Calabro, Italy, 2022, pp. 1-4.

[15] S. N. Azemi, K. Ghorbani and W. S. T. Rowe, "A Reconfigurable FSS Using a Spring Resonator Element," in *IEEE Antennas Wireless Propag. Lett.*, vol. 12, pp. 781-784, 2013.

[16] D. Ferreira, I. Cuiñas, R. F. S. Caldeirinha and T. R. Fernandes, "3-D Mechanically Tunable Square Slot FSS," *IEEE Trans. on Antennas and Propag.*, vol. 65, no. 1, pp. 242-250, Jan. 2017.

[17] M. Mantash and T. A. Denidni, "3D FSS polarizer for millimeter-wave antenna applications," *International Journal of RF and Microwave Computer-Aided Engineering*, vol. 29, no. 8, Aug. 2019.

[18] B. Li and Z. Shen, "Three-Dimensional Bandpass Frequency-Selective Structures With Multiple Transmission Zeros,", *IEEE Trans. on Microwave Theory and Techn.*, vol. 61, no. 10, pp. 3578-3589, Oct. 2013

[19] B. Sanz-Izquierdo and E. A. Parker, "3-D Printing of Elements in Frequency Selective Arrays," *IEEE Trans. on Antennas and Propag.*, vol. 62, no. 12, pp. 6060-6066, Dec. 2014.

[20] Arrow Staples UK, "Arrow Staples UK," 2025. [Online]. Available: https://www.arrowstaples.co.uk/. [Accessed: Apr. 16, 2025].

[21] H. Saghlatoon, L. Sydänheimo, L. Ukkonen and M. Tentzeris, "Optimization of Inkjet Printing of Patch Antennas on Low-Cost Fibrous Substrates," in *IEEE Antennas and Wireless Propagation Letters*, vol. 13, pp. 915-918, 2014.

[22] K. Sarabandi and N. Behdad, "A Frequency Selective Surface With Miniaturized Elements," *IEEE Trans. on Antennas and Propag.*, vol. 55, no. 5, pp. 1239-1245, May 2007.

[23] R. J. Langley and E. A. Parker. (1982) Equivalent circuit model for arrays of square loops. Electronics Letters, 18 (7). pp. 294-296. ISSN 0013-5194.

[24] Marcuwitz, N.: 'Waveguide handbook' (McGraw-Hill, USA, 1951, 1st edn.)

[25] F. Costa, A. Monorchio, and G. Manara, "An overview of equivalent circuit modeling techniques of frequency selective surfaces and metasurfaces," *ACES J.,* vol. 29, no. 12, pp. 960–976, Dec. 2014.

[26] F. Conde-Pumpido, G. Perez-Palomino, J. R. Montejo-Garai and J. E. Page, "Generalized Bimode Equivalent Circuit of Arbitrary Planar Periodic Structures for Oblique Incidence," in *IEEE Transactions on Antennas and Propagation*, vol. 70, no. 10, pp. 9435-9448, Oct. 2022.

[27] G. H. H. Sung, K. W. Sowerby and A. G. Williamson, "The impact of frequency selective surfaces applied to standard wall construction materials," *IEEE Antennas Propag. Soc. Int. Symp., 2004.*, Monterey, CA, USA, 2004, pp. 2187-2190 Vol.2.

[28] M. Raspopoulos and S. Stavrou, "Frequency selective surfaces on building materials – air gap impact," *Electron. Lett.*, vol. 43, no. 13, pp. 731–732, Jun. 2007.

[29] S. S. Zhekov, O. Franek and G. F. Pedersen, "Dielectric Properties of Common Building Materials for Ultrawideband Propagation Studies [Measurements Corner]," *IEEE Antennas and Propag. Mag.*, vol. 62, no. 1, pp. 72-81, Feb. 2020.

[30] Y. Pinhasi, A. Yahalom and S. Petnev, "Propagation of ultra wide-band signals in lossy dispersive media," *2008 IEEE International Conference on Microwaves, Communications, Antennas and Electronic Systems*, Tel-Aviv, Israel, 2008, pp. 1-10.